Doping of semiconductor nanowires

Jesper Wallentin[a)] and Magnus T. Borgström
Division of Solid State Physics, Lund University, SE-221 00 Lund, Sweden

(Received 28 January 2011; accepted 31 May 2011)

A cornerstone in the successful application of semiconductor nanowire devices is controlled impurity doping. In this review article, we discuss the key results in the field of semiconductor nanowire doping. Considerable development has recently taken place in this field, and half of the references in this review are less than 3 years old. We present a simple model for dopant incorporation during in situ doping of particle-assisted growth of nanowires. The effects of doping on nanowire growth are thoroughly discussed since many investigators have seen much stronger and more complex effects than those observed in thin-film growth. We also give an overview of methods of characterizing doping in nanowires since these in many ways define the boundaries of our current understanding.

I. INTRODUCTION

Semiconductor nanowires (NWs) have emerged as one of the most powerful and versatile building blocks for integration of nanoscale devices with current technology. The geometry of NWs permits efficient strain relaxation, which in turn allows the combination of materials not normally compatible, as well as the growth of III–V NWs on Si.[1,2] Numerous technically and scientifically interesting devices have been demonstrated using NWs, such as field effect transistors (FETs),[3] single-electron transistors,[4] and spin-orbit qubits.[5]

Doping is necessary in most device applications to control the conductivity of the NWs. Doping of semiconductor NWs was first investigated almost two decades ago by the pioneering group of Hiruma, who demonstrated GaAs p–n junctions.[6] Interest in NWs developed rapidly after Lieber's group demonstrated controlled doping in Si NWs,[7] and successful doping has since then enabled fabrication of photovoltaic devices,[8] single-quantum-dot light-emitting diodes,[9] and tunneling FETs.[10] The rapid development of the field of NW doping is demonstrated by the fact that about half of the references in this review were published during the past 3 years.

Despite these advances, many challenges remain in both understanding and controlling the doping of NWs. The size of NWs prevents the use of standard Hall measurements to determine doping levels, and the evaluation of carrier concentrations and mobilities remains difficult. The dynamics of NW growth is complex, even without considering doping, and, as discussed in a special section, the effects of doping are often much stronger than in thin-film growth. Furthermore, NWs are often grown at significantly lower temperatures than thin films, for which an understanding of doping has been developed.[11] While the non-nitride III–V semiconductors grow in the cubic zincblende (ZB) form in bulk, III–V NWs commonly exhibit a mixture of ZB and the lower symmetry, hexagonal wurtzite (WZ) crystal structure. This polytypism has been the focus of much research during recent years,[12] and the crystal structure can to some extent be controlled by growth conditions such as temperature and V/III ratio. Interestingly, it has also been found that doping can strongly affect the crystal structure of III–V NWs.[13,14]

There are many requirements for doping of semiconductor NWs. Obviously, it must be possible to achieve suitable high carrier concentrations, and, as will be discussed later, there are good reasons to believe that higher dopant concentrations than in bulk will be needed in NWs. For commercial applications, the doping method should allow large-scale production at a reasonable cost. The spatial distribution of the dopants must also be sufficiently controlled for the application. For instance, the position of a single dopant atom may strongly affect the performance of FETs at gate lengths below 10 nm.[15]

Since NWs are typically grown vertically on the substrate, it is natural to define devices and therefore doping profiles vertically, in contrast to traditional planar devices. A vertical geometry poses special challenges for diffusion and ion implantation, the two currently dominating doping methods for planar devices. Since the NWs discussed in this review are based on epitaxial growth, it is attractive to introduce dopants during growth, and we will therefore mainly discuss in situ doping in this review.

Below, we discuss the mechanisms, growth effects, and measurements of doping of epitaxially grown semiconductor NWs, rather than the applications. We focus on the doping of NWs grown using the popular vapor–liquid–solid

[a)]Address all correspondence to this author.
e-mail: jesper.wallentin@ftf.lth.se
DOI: 10.1557/jmr.2011.214

 © Materials Research Society 2011

https://doi.org/10.1557/jmr.2011.214 Published online by Cambridge University Press

TABLE I. Table of references regarding in situ doping of semiconductor NWs.

Material	n-type	p-type	Other
Si	P,[7] PH_3,[10,16–24] TMSb[25]	B_2H_6,[7,10,19,26–28] TMB,[18,28] AsH_3,[18] $AsCl_3$,[29] Al (as seed)[30]	$NdCl_3$,[31] O_2[32]
Ge, SiGe	PH_3,[33–37] Sb[38]	B_2H_6,[27,33–36,39,40] $AsCl_3$[29]	Mn[41]
SiC	$AlCl_3$[42]		
AlN			$MnCl_2$[43]
GaN	Si,[44–47] SiH_4[48]	Mg_3N_2,[49,50] Cp_2Mg,[48] Mg,[45–47,51] $MgCl_2$,[52] Hg[53]	$MnCl_2$[54,55]
GaP	S[56]	NH_3[57]	Mn[58]
GaAs	Si,[59–61] SiH_4,[62] Si_2H_6,[6,63] GaTe,[64,65]	Si,[61,66,67] TMGa,[6] DEZn,[62,68,69] Be,[60,64,65]	Mn (as seed)[70]
InN	Si[71,72]	DEZn,[73] Mg[72]	
InP	Si,[74] SiH_4,[75] Te,[76] TESn,[77] H_2S,[69,78,79] Se[80,81]	Zn,[76,81] Zn_3P_2,[82] DMZn,[77] DEZn[14,75,78,83,84]	
InAs	$SiBr_4$,[85] TESn,[85] H_2S,[85] DTBSe[85]	Be[86]	
ZnO	ZnS,[87] S,[88] SnO_2,[89] NH_3,[90] Ga_2O_3,[91] In_2O_3[13]	B,[92] P_2O_5,[93,94] N_2O,[95] NaCl[96]	$MnCl_2$,[97,98] $Mn_x(CO)_y$[99] Review: Refs. 100 and 101
In_2O_3	SnO[102–104]		
SnO_3	In_2O_3,[105] Sb,[106] Sb_2O_3[107]		
II–VI			Review: Ref. 108

(VLS) method, but other methods of growth are discussed as well. Most of the pioneering work in NW growth using the VLS method has been done with gold as the seed material, and this is also reflected in this review. We have mainly reviewed intentional doping with the purpose of modifying the carrier concentration although we also include some other types of doping.

We first present a table of references regarding in situ doping of NWs. This is followed by a qualitative model for dopant incorporation during in situ doping and the discussion of some of the key results in this field. The effects of doping on NW growth have received increasing attention during recent years and thus warrant a special section. Thereafter, other methods used for NW doping are discussed. Finally, we present an overview of methods that have been used for characterization of doping in NWs.

II. IN SITU DOPING REFERENCE LIST

In Table I, we present a comprehensive but not exhaustive list of references to articles concerning in situ doping of semiconductor NWs, sorted according to the NW material.

III. INCORPORATION DURING IN SITU DOPING

In this section, we present a qualitative model for doping during VLS growth of NWs and discuss key results in this area. There are numerous publications concerning undoped NW growth, and two recent reviews can be found in Refs. 109 and 110. We assume here that the NWs are grown from a liquid metal seed particle and that the growth material and the dopant precursors are supplied from the vapor phase. Apart from axial growth, which creates the NWs, there is normally also radial growth, often leading to a tapered shape, as well as competitive substrate growth (indicated in Fig. 1).

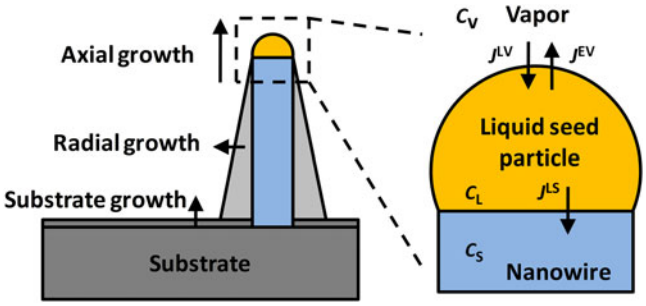


FIG. 1. Schematic of the concentrations and fluxes of dopant in vapor–liquid–solid nanowire (NW) growth.

Dopants may enter the NW in the axial growth via the seed particle or via the particle–NW interface. Several authors have found dopant incorporation to be more efficient in the radial growth than in the axial growth.[66,111] The dopants may be incorporated in the radial growth via adsorption and capture. Some dopants have high solid diffusivity and may possibly diffuse into the NW from the side facets. Conversely, it is also possible that dopants may leave the crystal via diffusion from the side facets if the dopant source is turned off.

Nonintentional radial overgrowth is usually undesirable as it can disturb the performance of axially defined devices. Tapering can be reduced by adjusting the growth conditions,[112] and it has been shown that in situ etching can completely prevent tapering in NW growth.[113] The radial incorporation of dopants is probably well described by established thin-film growth models although the

https://doi.org/10.1557/jmr.2011.214 Published online by Cambridge University Press

unusual side facets and growth temperatures must be taken into consideration. We therefore mainly discuss the incorporation of dopants in the axial growth.

Our model is influenced by the boundary-layer model developed by Stringfellow for doping in thin-film metal organic vapor phase epitaxy (MOVPE).[11] Consider a NW growing at steady state. The concentrations of dopant are c_V, c_L, and c_S, in the vapor, liquid, and solid, respectively (see Fig. 1). The fluxes of dopant are J^{LV}, from the vapor into the liquid, J^{LS}, from the seed particle into the crystal, and J^{EV}, reevaporation from the liquid into the vapor. The flux of seed metal into the crystal is assumed to be negligible.

We assume that doping at the interface locally occurs as in a liquid-phase epitaxy (LPE) system, as recently suggested by Dufouleur et al.[66] The segregation coefficients here may differ from those established in regular LPE, due to the presence of the seed metal. We note that the segregation coefficients established in regular LPE show considerable variation between different dopants for the same host material and between different host materials for the same dopant. For instance, LPE of InP shows dopant segregation coefficients that vary from 30 for Si to 2×10^{-3} for Sn.[114]

Two extreme types of dopants can be identified:

Type A: For a dopant with low solubility in the seed particle but high segregation coefficient into the solid, the dopants will be depleted out of the seed particle and the concentration c_L will be low. The reevaporation, J^{EV}, will therefore also be negligible, which means that $J^{LV} = J^{LS}$.

Type B: Conversely, if the dopant has high solubility in the seed particle but a low segregation coefficient for solid incorporation, the reevaporation J^{EV} will be significant and much larger than J^{LS}. The steady-state concentration c_L will be determined by the thermodynamic phase diagram of the liquid–vapor system. The solid concentration is given by the segregation coefficient k, defined by $c_S = k\, c_L$.

A typical type A dopant seems to be P in the doping of Ge and Si NWs using Au seed particles. Schmid et al.[20] investigated P doping of Si NWs and found that the concentration could be increased continuously with the molar fraction of phosphine (PH_3) until the solid solubility limit of P in Si was reached. An example of a type B dopant is Sb doping in the Au-seeded growth of Ge, where the liquid particle has recently been observed in situ using transmission electron microscopy to contain several tens of percent of Sb.[38] Another example is Si doping of Ga-seeded GaAs NWs,[66] which is interesting since it is probably one of the few systems for which relevant data on the distribution coefficient can be found.

The model described here can be compared with Stringfellow's, where he considered a boundary-layer model and distinguished between case I and case II dopants depending on their vapor pressure.[11] The case I dopant, with low vapor pressure, would correspond to the type A dopant defined here, while the case II, with high vapor pressure, would correspond to the type B dopant. Case I is also the kinetically limited case, where mass transport of the dopant governs the solid concentration. Perea et al.[21] investigated P doping of Au-seeded Ge NWs. Using mass transport arguments, they concluded that in this case the concentration of dopant in the solid was given by the ratio of fluxes into the seed particle. However, the solid concentration is not necessarily equal to the ratio of the fluxes or molar fractions in the vapor phase since the diffusion lengths, decomposition rates, and sticking coefficients may be different for the dopant and the growth precursor. Case II is the thermodynamically limited case, where reevaporation dominates and mass transport arguments are inadequate.

Note that in VLS growth it is not the vapor pressure in the vapor–solid system that determines which category a dopant belongs to, but a combination of the liquid–vapor thermodynamics and the liquid–solid segregation coefficients, as described earlier. For example, consider sulfur doping of InP. S has a high vapor pressure and is therefore considered a case II dopant in thin-film growth. In NW growth, S has low solubility in liquid metals but can be efficiently incorporated into InP[115] and is therefore probably a type A dopant. Some other typical n-dopants such as P and As (for group IV NWs) can also be expected to show type A behavior since they have low solubility in liquid metals. Most other dopants have high solubility in metals, but their segregation coefficients vary considerably and are generally unknown for relevant conditions.

The solubility of the dopants in the seed particle can be expected to have a strong influence on the gradient when the dopant source is turned on or off, and the steady state assumption is no longer valid. This gradient can be of critical importance for devices such as FETs. For type A dopants, it should in principle be possible to achieve gradients as sharp as those achieved in thin-film growth. Diffusion through a liquid seed particle is expected to be fast and should not limit the dopant incorporation. In support of this assumption, Schmid et al.[20] found a diameter-independent P incorporation in Si NWs and demonstrated 30-nm-short doped segments. For type B dopants, the dopants will be stored in the seed particle and the expected gradient should be less abrupt.

Although these nonsteady-state effects are difficult to investigate thoroughly for doping because of the difficulty in performing accurate measurements, comparisons can be made with NW heterostructures that have been studied in great detail. A theoretical comparison was made by Li et al.[116] Group V elements in III–V NWs have similarly low solubility as type A dopants, and very abrupt InAs–InP heterostructures have been observed using chemical beam epitaxy (CBE).[117] In MOVPE, the gradient becomes limited by reactor memory effects,[118] similar to the case in thin films. By contrast, Si and Ge as well as group III elements have high solubility, like the type B

https://doi.org/10.1557/jmr.2011.214 Published online by Cambridge University Press

dopants, and when switching these elements, the heterostructure gradients are on the order of the NW diameter.[69,116] For the growth components, the consumption of material out of the seed particle is naturally on the same order as the growth rate, but for dopants, the segregation coefficient should also be considered. With low segregation coefficients, the consumption of dopant will be low and the memory effects in principle long. However, the dopants often have a much higher vapor pressure than the group III or IV growth precursors, and reevaporation could reduce the memory effects significantly. The sharpness of doping profiles can be examined by creating Esaki tunnel diodes, which require p-n junctions with a depletion width on the order of 10 nm for successful operation. Our group was able to demonstrate efficient tunnel diodes, despite NW diameters and InP–GaAs heterojunction gradients of almost 100 nm.[69] Techniques that have been used for heterointerfaces and which could be explored for sharp doping gradients are growth interrupts,[118,119] where one element is purged from the seed particle before turning on the new one, and growth from solid seed particles,[120] which exploits the much lower solubility in the solid state.

For compound semiconductors, the relative fluxes or partial pressures of the anions and cations must be considered. It is well known in thin-film growth that, for example, a relatively low AsH_3 flow enhances S incorporation in GaAs[11] since S is incorporated on group V lattice sites. Although the V/III ratio in the vapor may be quite high, the ratio in the seed particle is normally much lower since the group V elements have lower solubility. Indeed recent experiments suggest that the group V element supersaturation could be growth limiting.[121] The low local V/III ratio suggests that p-type doping of III–V NWs would be more difficult than in thin films, but, as discussed earlier, the solubility of p-type dopants in the seed particle is typically much higher than that of n-type dopants. These effects are critical when using amphoteric dopants, which can induce n- or p-type doping depending on which lattice site they occupy. Colombo et al.[61] showed that the type of doping achieved by Si doping of GaAs NWs depends on the growth conditions, and they used this to create a p–i–n structure using only Si as dopant.

In MOVPE, the dopants are introduced via molecular precursors rather than as elements. Depending on the growth temperature and the precursor, the decomposition of the dopant precursor must be considered. For instance, silane pyrolysis is not complete even at bulk growth temperatures of GaAs; therefore, Si doping increases with temperature.[11] Since the growth temperature for NWs is often 100–300 °C below that of the corresponding thin films, pyrolysis may be important for precursors that are completely cracked in thin-film growth. Our group has investigated both DMZn[77] and DEZn[83,84] as p-type dopants of InP, shown in Fig. 2. Using DEZn, we found a growth rate that was independent of the DEZn molar fraction, while DMZn strongly increased the growth rate (as discussed in more detail in the next section). We attributed this difference to the higher decomposition temperature of DMZn as the undecomposed DMZn precursor could act as a surface passivator suppressing competitive thin-film growth. If the dopant precursors are not fully decomposed, catalytic decomposition on the seed particle surface as well as heterogeneous reactions should also be considered.

NWs have a large surface-to-volume ratio, which may influence dopant incorporation. Theoretical investigations

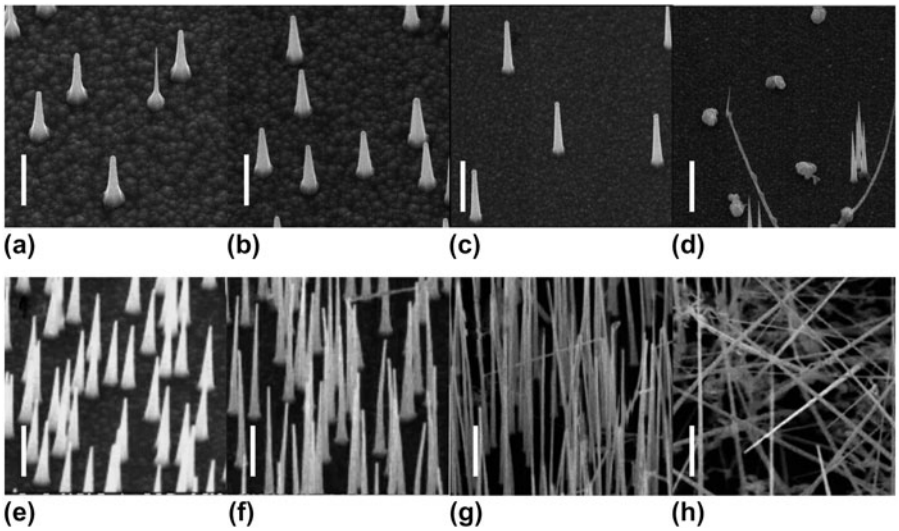


FIG. 2. Growth effects of InP NWs doped with varying molar fractions (χ) of (a)–(d) DEZn and (e)–(h) DMZn: (a) $\chi_{DEZn} = 0$ (ref), (b) $\chi_{DEZn} = 0.7 \times 10^{-6}$, (c) $\chi_{DEZn} = 10.7 \times 10^{-6}$, (d) $\chi_{DEZn} = 21.4 \times 10^{-6}$, (e) $\chi_{DMZn} = 1 \times 10^{-6}$, (f) $\chi_{DMZn} = 9.8 \times 10^{-6}$, (g) $\chi_{DMZn} = 48.7 \times 10^{-6}$, and (h) $\chi_{DMZn} = 97.5 \times 10^{-6}$. Tilt 30° to the normal. Scale bars 1μm.

https://doi.org/10.1557/jmr.2011.214 Published online by Cambridge University Press

have predicted that it will be energetically favorable for dopants to segregate to the surface[122,123] although these calculations were performed for few-nanometer-diameter NWs with much higher surface-to-volume ratio than typical NWs. Xie et al.[124] investigated doped Si and Ge NWs experimentally and found a "transition diameter" of around 22 nm. Below this diameter, the doping in the bulk of the NW was low and most of the dopants were found in a surface layer, while for NWs with larger diameter, there was significant bulk doping together with a highly doped shell. The authors explained this in terms of a fixed number of surface states to which the dopants could segregate. Above the transition diameter, the surface-to-volume ratio would be sufficiently small for all these states to be occupied, thus allowing for effective bulk doping. In this context, it is important to bear in mind that it is also possible that dopants could leave the crystal via diffusion and desorption from the side facets. If such a process would be efficient, a lower-doped surface would be expected instead; however, to the best of our knowledge, this has not been observed experimentally.

Although thermodynamic arguments are important, NWs are by shape and definition not in the lowest energy state. It is, for instance, well established that the crystal structure of NWs is governed by kinetics rather than thermodynamics.[125] NW growth rates are usually significantly higher than those of regular thin films, which can have implications for dopant incorporation. For instance, Zn doping of thin-film InP is more effective at higher growth rates.[126]

So far, the incorporation of dopants rather than carrier generation has been considered. In thin films, most dopants can safely be assumed to be ionized at room temperature. Theoretical predictions[127] and experiments[128] have shown that the ionization energy of dopants increases in thin NWs because of electrostatic effects. As discussed earlier, there can be a tendency for dopants to segregate at the surface, and this raises the question of whether these dopants will generate carriers or be neutralized. Theoretical work has suggested that the dopants will be passivated,[129] but there is experimental evidence of electrically active dopants at the surface.[124] These could provide high carrier concentrations while the mobility-limiting ions would reside away from the channel where carrier transport takes place, similar to the remote doping used for high-mobility 2DEGs.

Despite all the complex mechanisms discussed earlier, the overall tendency seems to be that NWs can be doped to similar levels as the corresponding thin films. Although accurate determination of doping levels is challenging, indirect evidence of high doping can be found in the performance of devices such as tunnel diodes[69] and tunnel-FETs,[10] as well as the nanosized ohmic contacts formed to many NWs.

IV. EFFECTS OF IN SITU DOPING ON NANOWIRE GROWTH

While in situ doping can affect thin-film growth by, for instance, step bunching, it can have quite dramatic effects on the growth of NWs. In this section, we will first discuss structural and morphological effects. Givargizov[29] reported periodic instabilities and faceting during growth of undoped Si and Ge NWs as early as 1973. He found that small additions of $AsCl_3$ prevented these instabilities and also observed that this dopant precursor improved the wetting of the seed particle. Much later, periodic faceting and periodic twinning were observed in In-doped ZnO NWs[13] [see Fig. 3(a)]. Similarly, Li et al.[19] reported that diborane induced saw-tooth faceting on the sidewalls of Si NWs [see Fig. 3(b)], unlike undoped and PH_3-doped segments which were smooth. When growing undoped segments followed by diborane-doped segments, they observed that faceting also developed on the undoped segments. This demonstrated that in this case the faceting developed during the radial overgrowth. Algra et al.[14] reported that undoped InP NWs grew with a mixed crystal structure, but that the addition of DEZn induced growth in a pure ZB crystal structure with rotational twins [see Fig. 3(c)]. Higher DEZn flows created a so-called twinning superlattice in which the distance between the twins was highly regular. These results were explained by changes in the surface energies of the seed particle, but no changes in contact angle between the seed particle and NW were found. Our group has recently investigated the same precursor, and we also observed a gradual transition to ZB structure with

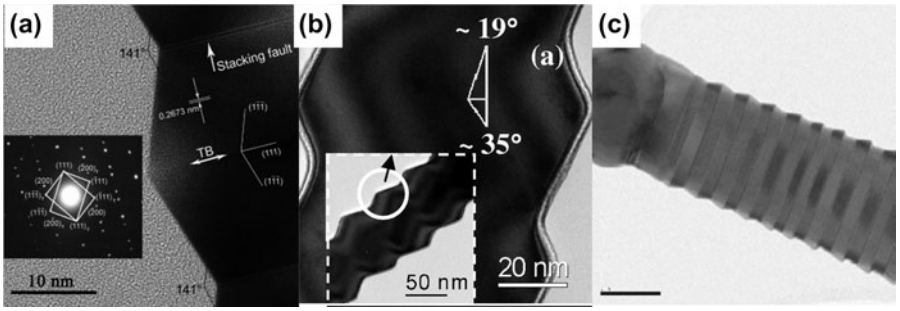


FIG. 3. Crystal structure effects in doped nanowires: (a) ZnO NWs doped with In_2O_3. (Adapted from Ref. 13, with permission from the American Chemical Society.) (b) Si NW doped using diborane. (Adapted from Ref. 19, with permission from the American Institute of Physics.) (c) InP NW doped with DEZn, scale bar 50 nm. (Adapted from Ref. 14, with permission from Nature Publishing Group.)

https://doi.org/10.1557/jmr.2011.214 Published online by Cambridge University Press

twinning.[83] In contrast to the results of Algra et al., we reported strong effects on the wetting of the seed particle. In line with the observations by Givargizov, we found that the periodic twinning correlated with a poor wetting of the seed particle although DEZn had the opposite effect of $AsCl_3$. We have previously shown a transition to ZB structure with twinning in InP NWs grown with DMZn,[77] which indicates that Zn, rather than the precursors, is responsible for the change in crystal structure. Effects on crystal structure from in situ doping have also been observed in GaN.[130]

The addition of dopants often affects the growth rate of NWs, both axially and radially. Lauhon et al. found that doping Si NWs with diborane created an amorphous Si shell,[27] but the shell could be made crystalline by high-temperature annealing. The reason for the radial overgrowth is that diborane improves the decomposition of silane, thereby enhancing film growth. Similarly, Tutuc et al.[40] reported that diborane strongly increased the radial growth of Ge NWs. Lew et al.[28] compared diborane with trimethylboron and observed no amorphous shell in the latter case. This effect was attributed to the higher stability of trimethylboron.

In contrast to the complex behavior of diborane, the n-dopant PH_3 has not shown strong effects on Si NW growth.[16,22] Schmid et al.[20] found that PH_3 had a minimal effect on the growth rate, but at sufficiently high concentrations, NW growth was completely inhibited. It has previously been observed that the addition of AsH_3[18] or TMSb[25] can suppress Si NW growth. Schmid et al. were also able to create n-type segments as short as 30 nm, demonstrating the limited memory effects and radial growth of this precursor. By contrast, Tutuc et al.[37] reported that phosphorus incorporates mainly in a radial shell for Ge NW growth.

We have studied the growth rates of InP NWs grown with DMZn[77] and DEZn.[83] As shown in Fig. 2, DMZn significantly increased the growth rate, while DEZn had little effect on the growth rate. The difference was attributed to the higher pyrolysis temperature of DMZn, which could allow the precursor to act as a surface passivator for radial growth. At very high molar fractions, we found that DEZn completely prevented InP NW growth. By contrast, it has been shown that the n-dopant H_2S induces perfect WZ crystal structure in InP NWs,[79] in agreement with previous indications.[78,84] H_2S also increases the axial growth rate and reduces the radial growth rate,[79,84] which is not surprising given that sulfur is a known surface passivator for InP. Rigutti et al.[74] found that Si doping of InP NWs increased the tapering and reduced the growth rate.

Thelander et al.[85] investigated the effect of several doping precursors on InAs NW growth using both MOVPE and CBE. They observed an increased ZB content because of Se doping of InAs, using DTBSe both in CBE and MOVPE. At high DTBSe flows in MOVPE, the NWs were pure ZB without twins and had a triangular cross section. These NWs exhibited strong radial growth with a 3% Se concentration. Using $SiBr_4$ in CBE, they found that this dopant induced growth of a doped shell, similar to the observations by Rigutti et al.[74] Finally, doping of GaN NWs has been found to have strong effects on growth and faceting.[51,55,131]

To summarize this section, in situ doping of NWs has in many cases been shown to have greater and more complex effects on NW growth than in the corresponding thin films. The effects of doping on, for example, growth rate and crystal structure are often stronger than the effects of changes in growth parameters such as V/III ratio. While some of these effects can be problematic, others such as higher crystal purity or decreased radial growth can be advantageous for applications.

V. OTHER DOPING METHODS

The two traditional methods of doping semiconductors, diffusion and ion implantation, have also been explored for NW doping, but to a lesser extent than in situ doping. For laterally defined devices, it can be cumbersome to position dopants in situ with epitaxy, but for vertical NW-based devices it instead the traditional methods that have geometrical challenges. Being nonequilibrium methods, they can in principle offer very high doping levels. Ford et al. were successful in carrying out challenging p-type doping in InAs NWs, using diffusion doping with Zn,[132] while others have investigated Si NWs.[133] Ho et al.[134] took advantage of the geometry and crystallinity of NWs by depositing a monolayer of dopant-containing molecules and demonstrated controlled p- and n-type doping of Si NWs after high-temperature annealing. Dharra et al. used Ga ions to n-type doped GaN NWs,[135] and others have explored ion implantation for Si[136,137] and GaAs[138] NWs. Colli et al.[139] investigated ion implantation of Si NWs in more detail and found that implantation induced limited amounts of structural disorder, which could be removed by annealing at 800 °C. Others have reported implantation of Si NWs standing as-grown.[140,141]

Several other methods of doping NWs have been explored. The reason for doping in most applications is to increase the carrier density, while the ionized dopants are unimportant or even detrimental to performance. Li et al.[142] used a doped InP shell to remotely p-dope an InAs core. Strain-induced polarization fields have been explored as a doping source in thin films,[143] and similar effects have been predicted in strained core-shell NWs.[144] Finally, stoichiometric control of N vacancies has been used to tune the carrier concentration in GaN NWs.[145,146]

VI. METHODS OF EVALUATING DOPING IN NANOWIRES

Our understanding of NW doping is closely related to our ability to evaluate the doping. Traditional Hall measurements have not been used because of the small

https://doi.org/10.1557/jmr.2011.214 Published online by Cambridge University Press

size of NWs. Quantitative doping measurements are still a major challenge in NW research although there has been a considerable development in recent years. Electrical measurements have historically been the most important, but recently many groups have demonstrated quantitative measurements using other techniques.

A. Electrical methods

The most commonly used method for quantitative characterization of doping is to create so-called nanowire field-effect transistor (NW-FET)[7] devices, shown in Fig. 4. These consist of a NW which has been broken off the growth substrate, placed on an insulating substrate, and contacted on both ends. The conductivity of the NW can be measured by sweeping the source–drain voltage and measuring the current. The conductivity, σ, is related to the carrier concentration n as[147]

$$\sigma = nq\mu \quad , \tag{1}$$

where q is the elementary charge and μ is the carrier mobility. By changing the potential of the back gate in the substrate, the transconductance can be measured, which can be used to estimate the mobility. In the linear transistor regime, the transconductance g_m is related to the mobility μ[147]:

$$g_m = \left.\frac{dI_{SD}}{dV_G}\right|_{V_{SD}\,\text{constant}} = \frac{C\mu}{L^2} V_{SD} \quad . \tag{2}$$

Here, I_{SD} is the source–drain current of the NW-FET, V_{SD} and V_G are the source–drain and gate voltages, respectively, and L is the length of the active region. C is the capacitance, which is usually modeled as a metallic cylinder surrounded by a dielectric some distance from an infinite, flat metallic back gate, leading to the following expression[148]:

$$C = \frac{2\pi L \varepsilon_0 \varepsilon_r}{\cosh^{-1}\left(\frac{R+h}{R}\right)} \quad , \tag{3}$$

where ε_r is the relative dielectric constant, ε_0 is the vacuum permittivity, R is the NW radius, and h is the distance between the gate and the bottom edge of the NW. Improved electrostatic control can be achieved by using a top gate[27] or by creating a vertical transistor with a wrap gate.[149]

In principle, both the carrier concentration and the mobility can be accurately determined with this method. However, many assumptions have been made which lead to limitations of the described model, as discussed in detail by Wunnicke[150] and Khanal and Wu[151] First, the dielectric does not surround the NW, but is rather a thin film, which leads to a reduction in capacitance by about a factor of two. Second, Eq. (3) is based on the assumption of an electrostatically metallic NW, while the NW is in fact semiconducting. Khanal and Wu simulated the effective capacitance for different doping levels and found that for highly doped NWs this holds quite well. In the case of nonmetallic NWs, the field penetrates the NW and the

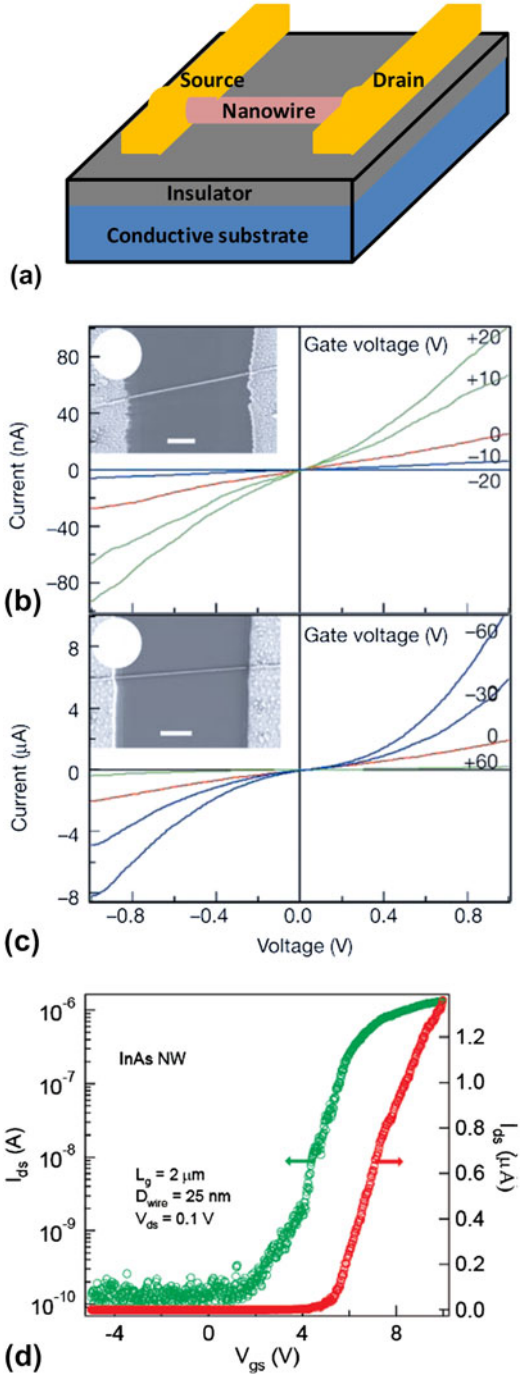


FIG. 4. Nanowire field-effect transistor (NW-FET) measurements. (a) Schematic of a NW-FET. (b) and (c) source–drain measurements of InP NWs doped with Te (b) and Zn (c). (Adapted from Ref. 76, with permission from Nature Publishing Group.) (d) Back gate-dependence of the source–drain current for an InAs NW-FET. (Adapted from Ref. 187, with permission from the American Chemical Society.)

https://doi.org/10.1557/jmr.2011.214 Published online by Cambridge University Press

charge distribution is far from uniform. Furthermore, the coupling depends on the carrier concentration, and the effective capacitance of low-doped samples can be less than half than of high-doped ones. An accurate model of the capacitance should also include the finite length of the NW[151] and screening by the source and drain contacts.[152]

A technical challenge associated with NW-FETs is making good electrical contacts. This can be difficult even with some bulk semiconductors, but NWs pose several additional problems. Theoretical models suggest that higher relative doping levels are needed in NW devices than in planar devices because of depletion.[153] Before metal deposition, any oxide should be removed, but because of the small size of the NWs, only gentle processing is possible. Additionally, many contact recipes developed for bulk semiconductors are based on high-temperature annealing, which leads to the formation of compounds and local drive-in of dopants that have been added to the metal layers. For example, a Pd/Zn/Pd/Au combination has been used for ohmic contacts to bulk p-type InP.[154] At a temperature of around 400 °C, Pd reacts with InP and the Zn is driven into the InP since the second Pd layer acts as a cap. However, in a nanometer-scale device such as an NW-FET, such reactions may lead to the entire device becoming metallic. The Zn may also diffuse out into the ambient rather than into the NW. Metals that are known to spike, that is, locally diffuse very deeply, such as Au and Ni, may also be problematic.

Despite these challenges, low-resistance ohmic contacts have been formed to NWs in many cases, for example, p-type[155] and n-type[16] Si, p-type[33,39] and n-type[33] Ge, p-type GaAs[68] and n-type InP,[76] and n-type[156] and p-type GaN.[52] It is of the utmost importance that the semiconductor is highly doped since this creates a thin Schottky barrier through which carriers may tunnel, although theoretical predictions suggest that this effect is reduced in thin NWs.[157] With reasonably good ohmic contacts, the contact resistance can be decoupled using transmission line measurements in which the channel length is varied. Four-point measurements can also be used to separate the contact resistance, but Thelander et al.[158] showed that for InAs NW-FETs with low-resistance contacts the inner probes were invasive. Lower-doped materials typically show nonlinear Schottky-like contacts.[77] Notably, InAs has a degenerate surface inversion layer, which allows ohmic contact formation even to nominally undoped material.

Without high-quality contacts to the NW, the resistance is normally limited by the contacts rather than the NW channel. Since the back gate affects the contacts and the NW channel simultaneously, poor contacts make the interpretation of both source–drain and gate–sweep measurements difficult. Zhang et al.[159] studied the source–drain characteristics of NW-FETs with nonohmic contacts in detail. Even without ohmic contacts, the gate–sweep measurements can be used to identify the type of majority carrier in the device (n- or p-type), and an estimate of the carrier concentration can be obtained from the threshold voltage.[77]

A strategy to circumvent the problems associated with contacts is to highly dope the ends of the NW while leaving the middle segment low-doped.[136,137] This type of structure can have very low contact resistance relative to the channel resistance and allows for devices with doping profiles more similar to planar MOSFETs. An extreme version of this concept was developed by Weber et al.,[160] who deposited Ni contacts on Si NWs and controllably transformed the ends to metallic $NiSi_2$ by annealing.

Overall, NW-FET measurements can often give precise data in terms of device resistance and transconductance. Converting these into quantitative material properties such as carrier concentration and mobility is straightforward, but the actual precision is often questionable because of the number of assumptions made.

Another electrical method involves capacitance–voltage (C–V) measurements, which, when used for thin films, typically utilizes a MOS structure. Information about the carrier density profile can be obtained by measuring the capacitance as a function of the gate voltage. C–V measurements on individual NWs were first demonstrated by Tu et al.[161] These measurements are difficult since the very low capacitances in NW devices are often hidden by much larger background capacitances, but by careful screening, the authors were able to estimate the mobility of Ge NWs. Roddaro et al. extended the C–V method to vertical devices,[162] using small arrays of NWs, and later estimated the carrier concentration as well as the surface state density.[163] Recently, this model was also used for studying doping incorporation in InAs NWs.[164] Garnett et al.[165] used lateral devices combined with theoretical modeling to estimate the radial distribution of carriers in Si NWs. Finally, Bakkers et al.[166] probed the resistivity of NWs by using a conductive atomic force microscopy tip put on NWs standing as-grown on the substrate.

B. Optical methods

Optical methods are attractive because they usually require no processing and may therefore be simpler and faster than electrical measurements. Although many authors have used photoluminescence (PL) and observed spectra that are characteristic of doped semiconductors, we concentrate here on optical methods intended for quantitative determination of the carrier concentration.

For highly doped semiconductors with low effective mass, the PL can be blue-shifted since the Fermi level shifts above the band edge, a so-called Burstein–Moss shift.[167] In a simple parabolic-band model, the shift is given by

https://doi.org/10.1557/jmr.2011.214 Published online by Cambridge University Press

$$\Delta E = \left(\frac{\hbar^2}{2m_{\text{eff}}}\right)(3\pi^2 n)^{2/3} \approx \frac{16.9}{m_{\text{eff}}}\left(\frac{n}{10^{19}\text{cm}^{-3}}\right)^{2/3}(\text{meV}) \quad . \tag{4}$$

However, the high carrier concentration also causes a red-shift because of band gap renormalization, which complicates the analysis. Bugajski and Lewandowski[167] measured and accurately modeled the peak position and peak width as functions of the carrier concentration in bulk n-doped InP, while Liu et al. found agreement between electrical and optical measurements for n-doped InP NWs.[81] For NWs grown in the bulk crystal structure, comparisons with published data or bulk reference samples should be able to give accurate estimates of the carrier concentration. Our group has recently observed PL shifted well into the visible region in InP NWs doped using H_2S,[79] although the doping also caused a transition to the WZ crystal structure for which bulk reference samples are not available.

Raman spectroscopy is another popular optical technique. Kawashima et al.[168] found that highly B-doped Si NWs exhibited a broadened signal toward the high–wave number side, which they attributed to a Fano resonance caused by interference between optical phonon Raman scattering and electric Raman scattering due to intra valence band hole excitation. They also observed a local vibrational mode of B incorporated into Si. Using modeling, they were able to estimate the carrier concentrations, and later these authors used the same technique to estimate the axial carrier distribution in single Si NWs.[26] Others have used Raman spectroscopy to study the doping of GaN,[169] InN,[72] and GaAs[60,67] NWs.

Parkinson et al.[170] pioneered the use of transient terahertz photoconductivity measurements for the analysis of NWs. This method is quite complex and relies on computer modeling for quantitative results. However, accurate information on not only the carrier concentration but also the mobility can be obtained. With a related technique, Richter et al.[171] and later Sanford et al.[172] used photoconductivity measurements of contacted GaN NWs to estimate the carrier concentration, mobility, and surface properties.

C. Mass spectrometric methods

Secondary-ion mass spectrometry (SIMS) is a standard technique for characterizing thin-film semiconductors. It offers extremely high sensitivity but it is a destructive method. The spatial resolution depends strongly on the details of the system used. Note that SIMS, unlike the electrical and optical techniques described earlier, measures the dopant concentration rather than the carrier concentration. Lew et al.[28] used SIMS to compare different B precursors for doping of Si NWs. Putnam et al.[173] investigated the radial distribution of the Au concentration in Au-seeded, micrometer-diameter wires and set an upper limit of 1.7×10^{16} atoms/cm^3.

Atom probe tomography (APT), shown in Fig. 5, is a development of SIMS in which a needle-shaped sample is exposed to pulsed electrical fields that remove ions by field emission. By combining time-of-flight measurements with array mass spectrometer detection, a three-dimensional reconstruction of the probed sample can be created. The detection limit can be lower than 10^{18} atoms/cm^3 and the spatial resolution can be in the sub-nanometer range. In principle, the original position of every ion detected—up to 50% of the ions emitted—can be determined. Perea et al. pioneered the use of APT for NW characterization,[174] and later studied Au incorporation[175] and dopant incorporation[21] in NWs. Others have studied B incorporation in Si NW.[176] In some ways, the combination of low detection limits and high spatial resolution makes APT the ultimate tool for characterization of doping, but it also has limitations. The process is relatively slow and only a part of the NW volume can be sampled. The technique requires elaborate sample preparation, such as growing NWs on

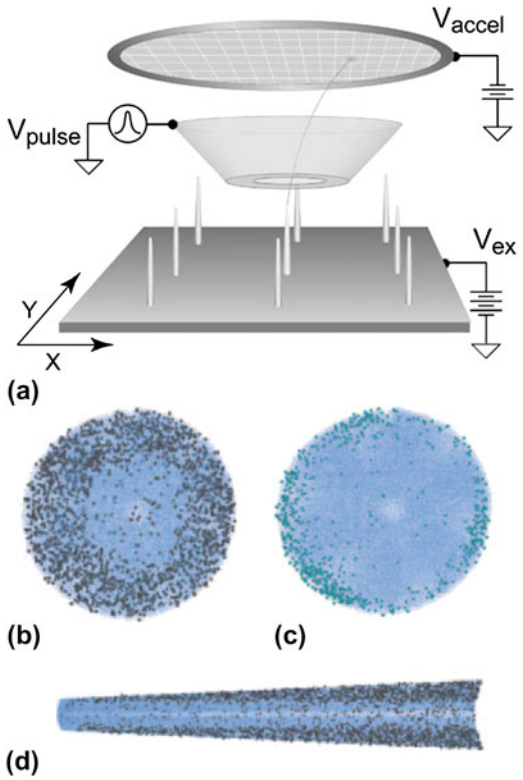


FIG. 5. Atom probe tomography (APT) of nanowires. (a) Schematic of APT instrument. (Adapted from Fig. 1 in Ref. 178, with permission from Springer Science+Business Media B.V.) (b, c) End-on view of Ge nanowire highlighting the distribution of (b) phosphorus (grey spheres) and (c) oxygen (light blue spheres) in germanium (blue dots). (d) Side view of nanowire cross section. [(b)–(d) Adapted from Ref. 21, courtesy of Nature Publishing Group.]

https://doi.org/10.1557/jmr.2011.214 Published online by Cambridge University Press

predefined pillars[176,177] or transferring NWs with a lift-out process using a micromanipulator and a focused ion beam.[178] For a recent review of APT analysis of semiconductors, see Ref. 180.

D. Scanning probe methods

Various scanning probe techniques have been used to investigate NW doping.[180–182] Scanning probe methods can have very high spatial resolution and are typically surface sensitive. Similarly to optical techniques, qualitative indications of doping can often be obtained, but quantitative measurements are more challenging. The doping of Si NW was quantitatively studied by Allen et al.[111] with scanning photocurrent microscopy (SPCM). Koren et al. used Kelvin probe force microscopy (KPFM) and successive etching steps to obtain the radial distribution of dopants in Si NWs,[183] and they also combined KPFM with SPCM to investigate the axial doping profile of Si NWs.[23] Scanning spreading resistance microscopy has also been used to measure the conductivity of NWs standing as-grown,[24] as well as in cross-section.[184] Finally, Stiegler et al.[185] investigated doped InP NWs with scattering-type scanning near-field optical microscopy.

E. Electron beam methods

Electron beam techniques such as energy dispersive x-ray spectroscopy are often standard techniques for the characterization of NW heterostructures. These have high spatial resolution but the relatively low sensitivity limits their use in characterizing doping. Our group has recently been able to detect Se in InAs NWs,[85] Zn in InP NWs,[83] and S in H_2S-doped InP NWs.[79] In the last case, the signal was strong enough to allow radial scans displaying increased signal at the surface of the NWs. Wang et al.[186] recently measured the Co distribution in ZnO NWs with electron energy loss spectroscopy.

VII. CONCLUSIONS

The doping of semiconductor NWs has seen tremendous development during the past years. The most promising results have been achieved with in situ doping, with which many materials have been successfully doped to levels similar to the corresponding thin films. Although much progress has been made in the measurement of NW doping, the fundamental understanding of NW doping is still hampered by the lack of simple and precise measurement methods. In situ doping has many strong and interesting effects on NW growth, effects which are sometimes greater than those achieved by tuning regular growth parameters. Although these effects further complicate the already complex area of NW growth, many authors have demonstrated successful devices using in situ doping.

ACKNOWLEDGMENTS

This work was performed within the Nanometer Structure Consortium at Lund University and was supported by the Swedish Research Council, the Swedish Foundation for Strategic Research, the Nordic Innovation Centre project Nanordsun, and the EU program AMON-RA (214814). This report is based on a project that was funded by E.ON AG as part of the E.ON International Research Initiative. The authors thank Claes Thelander and Knut Deppert for valuable discussions.

REFERENCES

1. T. Mårtensson, C.P.T. Svensson, B.A. Wacaser, M.W. Larsson, W. Seifert, K. Deppert, A. Gustafsson, L.R. Wallenberg, and L. Samuelson: Epitaxial III-V nanowires on silicon. *Nano Lett.* **4**, 1987 (2004).
2. E.P.A.M. Bakkers, M.T. Borgström, and M.A. Verheijen: Epitaxial growth of III-V nanowires on group IV substrates. *MRS Bull.* **32**, 117 (2007).
3. Y. Cui and C.M. Lieber: Functional nanoscale electronic devices assembled using silicon nanowire building blocks. *Science* **291**, 851 (2001).
4. C. Thelander, T. Mårtensson, M.T. Björk, B.J. Ohlsson, M.W. Larsson, L.R. Wallenberg, and L. Samuelson: Single-electron transistors in heterostructure nanowires. *Appl. Phys. Lett.* **83**, 2052 (2003).
5. S. Nadj-Perge, S.M. Frolov, E.P. Bakkers, and L.P. Kouwenhoven: Spin-orbit qubit in a semiconductor nanowire. *Nature* **468**, 1084 (2010).
6. K. Haraguchi, T. Katsuyama, K. Hiruma, and K. Ogawa: GaAs p-n junction formed in quantum wire crystals. *Appl. Phys. Lett.* **60**, 745 (1992).
7. Y. Cui, X.F. Duan, J.T. Hu, and C.M. Lieber: Doping and electrical transport in silicon nanowires. *J. Phys. Chem. B* **104**, 5213 (2000).
8. T.J. Kempa, B.Z. Tian, D.R. Kim, J.S. Hu, X.L. Zheng, and C.M. Lieber: Single and tandem axial p-i-n nanowire photovoltaic devices. *Nano Lett.* **8**, 3456 (2008).
9. E.D. Minot, F. Kelkensberg, M. van Kouwen, J.A. van Dam, L.P. Kouwenhoven, V. Zwiller, M.T. Borgström, O. Wunnicke, M.A. Verheijen, and E.P.A.M. Bakkers: Single quantum dot nanowire LEDs. *Nano Lett.* **7**, 367 (2007).
10. M.T. Björk, J. Knoch, H. Schmid, H. Riel, and W. Riess: Silicon nanowire tunneling field-effect transistors. *Appl. Phys. Lett.* **92**, 193504 (2008).
11. G.B. Stringfellow: The role of impurities in III/V semiconductors grown by organometallic vapor-phase epitaxy. *J. Cryst. Growth* **75**, 91 (1986).
12. P. Caroff, J. Bolinsson, and J. Johansson: Crystal phases in III–V nanowires: From random toward engineered polytypism. *IEEE J. Sel. Top. Quant. Electron.* **PP**, 18 (2010).
13. L.A. Xu, Y. Su, Y.Q. Chen, H.H. Xiao, L.A. Zhu, Q.T. Zhou, and S. Li: Synthesis and characterization of indium-doped ZnO nanowires with periodical single-twin structures. *J. Phys. Chem. B* **110**, 6637 (2006).
14. R.E. Algra, M.A. Verheijen, M.T. Borgström, L-F. Feiner, G. Immink, W.J.P. van Enckevort, E. Vlieg, and E.P.A.M. Bakkers: Twinning superlattices in indium phosphide nanowires. *Nature* **456**, 369 (2008).
15. N. Seoane, A. Martinez, A.R. Brown, J.R. Barker, and A. Asenov: Current variability in Si nanowire MOSFETs due to random

https://doi.org/10.1557/jmr.2011.214 Published online by Cambridge University Press

dopants in the source/drain regions: A fully 3-D NEGF simulation study. *IEEE Trans. Electron. Dev.* **56**, 1388 (2009).
16. G.F. Zheng, W. Lu, S. Jin, and C.M. Lieber: Synthesis and fabrication of high-performance n-type silicon nanowire transistors. *Adv. Mater.* **16**, 1890 (2004).
17. B.S. Kim, T.W. Koo, J.H. Lee, D.S. Kim, Y.C. Jung, S.W. Hwang, B.L. Choi, E.K. Lee, J.M. Kim, and D. Whang: Catalyst-free growth of single-crystal silicon and germanium nanowires. *Nano Lett.* **9**, 864 (2009).
18. H. Schmid, M.T. Björk, J. Knoch, H. Riel, W. Riess, P. Rice, and T. Topuria: Patterned epitaxial vapor-liquid-solid growth of silicon nanowires on Si(111) using silane. *J. Appl. Phys.* **103**, 024304 (2008).
19. F. Li, P.D. Nellist, and D.J.H. Cockayne: Doping-dependent nanofaceting on silicon nanowire surfaces. *Appl. Phys. Lett.* **94**, 263111 (2009).
20. H. Schmid, M.T. Björk, J. Knoch, S. Karg, H. Riel, and W. Riess: Doping limits of grown in situ doped silicon nanowires using phosphine. *Nano Lett.* **9**, 173 (2009).
21. D.E. Perea, E.R. Hemesath, E.J. Schwalbach, J.L. Lensch-Falk, P.W. Voorhees, and L.J. Lauhon: Direct measurement of dopant distribution in an individual vapour-liquid-solid nanowire. *Nat. Nanotechnol.* **4**, 315 (2009).
22. Y.F. Wang, K.K. Lew, T.T. Ho, L. Pan, S.W. Novak, E.C. Dickey, J.M. Redwing, and T.S. Mayer: Use of phosphine as an n-type dopant source for vapor-liquid-solid growth of silicon nanowires. *Nano Lett.* **5**, 2139 (2005).
23. E. Koren, Y. Rosenwaks, J.E. Allen, E.R. Hemesath, and L.J. Lauhon: Nonuniform doping distribution along silicon nanowires measured by Kelvin probe force microscopy and scanning photocurrent microscopy. *Appl. Phys. Lett.* **95**, 092105 (2009).
24. C. Celle, C. Mouchet, E. Rouviere, J.P. Simonato, D. Mariolle, N. Chevalier, and A. Brioude: Controlled in situ n-doping of silicon nanowires during VLS growth and their characterization by scanning spreading resistance microscopy. *J. Phys. Chem. C* **114**, 760 (2010).
25. P. Nimmatoori, Q. Zhang, E.C. Dickey, and J.M. Redwing: Suppression of the vapor-liquid-solid growth of silicon nanowires by antimony addition. *Nanotechnology* **20**, 025607 (2009).
26. G. Imamura, T. Kawashima, M. Fujii, C. Nishimura, T. Saitoh, and S. Hayashi: Distribution of active impurities in single silicon nanowires. *Nano Lett.* **8**, 2620 (2008).
27. L.J. Lauhon, M.S. Gudiksen, C.L. Wang, and C.M. Lieber: Epitaxial core-shell and core-multishell nanowire heterostructures. *Nature* **420**, 57 (2002).
28. K.K. Lew, L. Pan, T.E. Bogart, S.M. Dilts, E.C. Dickey, J.M. Redwing, Y.F. Wang, M. Cabassi, T.S. Mayer, and S.W. Novak: Structural and electrical properties of trimethylboron-doped silicon nanowires. *Appl. Phys. Lett.* **85**, 3101 (2004).
29. E.I. Givargizov: Periodic instability in whisker growth. *J. Cryst. Growth* **20**, 217 (1973).
30. B.A. Wacaser, M.C. Reuter, M.M. Khayyat, C.Y. Wen, R. Haight, S. Guha, and F.M. Ross: Growth system, structure, and doping of aluminum-seeded epitaxial silicon nanowires. *Nano Lett.* **9**, 3296 (2009).
31. W.F. Lee, C.Y. Lee, M.L. Ho, C.T. Huang, C.H. Lai, H.Y. Hsieh, P.T. Chou, and L.J. Chen: Nd-doped silicon nanowires with room temperature ferromagnetism and infrared photoemission. *Appl. Phys. Lett.* **94**, 263117 (2009).
32. S. Kodambaka, J.B. Hannon, R.M. Tromp, and F.M. Ross: Control of Si nanowire growth by oxygen. *Nano Lett.* **6**, 1292 (2006).
33. A.B. Greytak, L.J. Lauhon, M.S. Gudiksen, and C.M. Lieber: Growth and transport properties of complementary germanium nanowire field-effect transistors. *Appl. Phys. Lett.* **84**, 4176 (2004).
34. E. Tutuc, J. Appenzeller, M.C. Reuter, and S. Guha: Realization of a linear germanium nanowire p-n junction. *Nano Lett.* **6**, 2070 (2006).
35. S.T. Le, P. Jannaty, A. Zaslavsky, S.A. Dayeh, and S.T. Picraux: Growth, electrical rectification, and gate control in axial in situ doped p-n junction germanium nanowires. *Appl. Phys. Lett.* **96**, 262102 (2010).
36. D. Wang and H. Dai: Germanium nanowires: From synthesis, surface chemistry, and assembly to devices. *Appl. Phys. A* **85**, 217 (2006).
37. E. Tutuc, J.O. Chu, J.A. Ott, and S. Guha: Doping of germanium nanowires grown in presence of PH3. *Appl. Phys. Lett.* **89**, 263101 (2006).
38. E. Sutter and P. Sutter: Vapor-liquid-solid growth and Sb doping of Ge nanowires from a liquid Au-Sb-Ge ternary alloy. *Appl. Phys. A* **99**, 217 (2010).
39. D.W. Wang, Q. Wang, A. Javey, R. Tu, H.J. Dai, H. Kim, P.C. McIntyre, T. Krishnamohan, and K.C. Saraswat: Germanium nanowire field-effect transistors with SiO2 and high-kappa HfO2 gate dielectrics. *Appl. Phys. Lett.* **83**, 2432 (2003).
40. E. Tutuc, S. Guha, and J.O. Chu: Morphology of germanium nanowires grown in presence of B2H6. *Appl. Phys. Lett.* **88**, 043113 (2006).
41. V. Grossi, F. Bussolotti, M. Passacantando, S. Santucci, and L. Ottaviano: Mn doping of germanium nanowires by vapour-liquid-solid deposition. *Superlattices Microstruct.* **44**, 489 (2008).
42. H.J. Choi, H.K. Seong, J.C. Lee, and Y.M. Sung: Growth and modulation of silicon carbide nanowires. *J. Cryst. Growth* **269**, 472 (2004).
43. Y. Yang, Q. Zhao, X.Z. Zhang, Z.G. Liu, C.X. Zou, B. Shen, and D.P. Yu: Mn-doped AlN nanowires with room temperature ferromagnetic ordering. *Appl. Phys. Lett.* **90**, 092118 (2007).
44. J. Liu, X.M. Meng, Y. Jiang, C.S. Lee, I. Bello, and S.T. Lee: Gallium nitride nanowires doped with silicon. *Appl. Phys. Lett.* **83**, 4241 (2003).
45. M.S. Son, S.I. Im, Y.S. Park, C.M. Park, T.W. Kang, and K.H. Yoo: Ultraviolet photodetector based on single GaN nanorod p-n junctions. *Mater. Sci. Eng., C* **26**, 886 (2006).
46. W. Guo, M. Zhang, A. Banerjee, and P. Bhattacharya: Catalyst-free InGaN/GaN nanowire light emitting diodes grown on (001) silicon by molecular beam epitaxy. *Nano Lett.* **10**, 3355 (2010).
47. F. Furtmayr, M. Vielemeyer, M. Stutzmann, A. Laufer, B.K. Meyer, and M. Eickhoff: Optical properties of Si- and Mg-doped gallium nitride nanowires grown by plasma-assisted molecular-beam epitaxy. *J. Appl. Phys.* **104**, 074309 (2008).
48. F. Qian, Y. Li, S. Gradecak, D.L. Wang, C.J. Barrelet, and C.M. Lieber: Gallium nitride-based nanowire radial heterostructures for nanophotonics. *Nano Lett.* **4**, 1975 (2004).
49. Z.H. Zhong, F. Qian, D.L. Wang, and C.M. Lieber: Synthesis of p-type gallium nitride nanowires for electronic and photonic nanodevices. *Nano Lett.* **3**, 343 (2003).
50. G.S. Cheng, A. Kolmakov, Y.X. Zhang, M. Moskovits, R. Munden, M.A. Reed, G.M. Wang, D. Moses, and J.P. Zhang: Current rectification in a single GaN nanowire with a well-defined p-n junction. *Appl. Phys. Lett.* **83**, 1578 (2003).
51. F. Limbach, E.O. Schafer-Nolte, R. Caterino, T. Gotschke, T. Stoica, E. Sutter, and R. Calarco: Morphology and optical properties of Mg doped GaN nanowires in dependence of growth temperature. *J. Optoelectron. Adv. Mater.* **12**, 1433 (2010).
52. Y.B. Tang, Z.H. Chen, H.S. Song, C.S. Lee, H.T. Cong, H.M. Cheng, W.J. Zhang, I. Bello, and S.T. Lee: Vertically aligned p-type single-crystalline GaN nanorod arrays on n-type Si for heterojunction photovoltaic cells. *Nano Lett.* **8**, 4191 (2008).
53. S.M. Zhou: Near UV photoluminescence of Hg-doped GaN nanowires. *Physica E* **33**, 394 (2006).

https://doi.org/10.1557/jmr.2011.214 Published online by Cambridge University Press

54. D.S. Han, J. Park, K.W. Rhie, S. Kim, and J. Chang: Ferromagnetic Mn-doped GaN nanowires. *Appl. Phys. Lett.* **86**, 032506 (2005).
55. P.V. Radovanovic, K.G. Stamplecoskie, and B.G. Pautler: Dopant ion concentration dependence of growth and faceting of manganese-doped GaN nanowires. *J. Am. Chem. Soc.* **129**, 10980 (2007).
56. Z.G. Chen, L.N. Cheng, G.Q. Lu, and J. Zou: Sulfur-doped gallium phosphide nanowires and their optoelectronic properties. *Nanotechnology* **21**, 375701 (2010).
57. H.W. Seo, S.Y. Bae, J. Park, M.I. Kang, and S. Kim: Nitrogen-doped gallium phosphide nanowires. *Chem. Phys. Lett.* **378**, 420 (2003).
58. D.S. Han, S.Y. Bae, H.W. Seo, Y.J. Kang, J. Park, G. Lee, J.P. Ahn, S. Kim, and J. Chang: Synthesis and magnetic properties of manganese-doped GaP nanowires. *J. Phys. Chem. B.* **109**, 9311 (2005).
59. H.G. Lee, H.C. Jeon, T.W. Kang, and T.W. Kim: Gallium arsenide crystalline nanorods grown by molecular-beam epitaxy. *Appl. Phys. Lett.* **78**, 3319 (2001).
60. M. Hilse, M. Ramsteiner, S. Breuer, L. Geelhaar, and H. Riechert: Incorporation of the dopants Si and Be into GaAs nanowires. *Appl. Phys. Lett.* **96**, 193104 (2010).
61. C. Colombo, M. Heibeta, M. Gratzel, and A. Fontcuberta i Morral: Gallium arsenide p-i-n radial structures for photovoltaic applications. *Appl. Phys. Lett.* **94**, 173108 (2009).
62. K. Tomioka, J. Motohisa, S. Hara, K. Hiruma, and T. Fukui: GaAs/AlGaAs core multishell nanowire-based light-emitting diodes on Si. *Nano Lett.* **10**, 1639 (2010).
63. K. Sladek, V. Klinger, J. Wensorra, M. Akabori, H. Hardtdegen, and D. Grutzmacher: MOVPE of n-doped GaAs and modulation doped GaAs/AlGaAs nanowires. *J. Cryst. Growth* **312**, 635 (2010).
64. J.A. Czaban, D.A. Thompson, and R.R. LaPierre: GaAs core-shell nanowires for photovoltaic applications. *Nano Lett.* **9**, 148 (2009).
65. J. Caram, C. Sandoval, M. Tirado, D. Comedi, J. Czaban, D.A. Thompson, and R.R. LaPierre: Electrical characteristics of core-shell p-n GaAs nanowire structures with Te as the n-dopant. *Nanotechnology* **21**, 134007 (2010).
66. J. Dufouleur, C. Colombo, T. Garma, B. Ketterer, E. Uccelli, M. Nicotra, and A.F.I. Morral: P-doping mechanisms in catalyst-free gallium arsenide nanowires. *Nano Lett.* **10**, 1734 (2010).
67. B. Ketterer, E. Mikheev, E. Uccelli, and A. Fontcuberta i Morral: Compensation mechanism in silicon-doped gallium arsenide nanowires. *Appl. Phys. Lett.* **97**, 223103 (2010).
68. C. Gutsche, I. Regolin, K. Blekker, A. Lysov, W. Prost, and F.J. Tegude: Controllable p-type doping of GaAs nanowires during vapor-liquid-solid growth. *J. Appl. Phys.* **105**, 024305 (2009).
69. J. Wallentin, J.M. Persson, J.B. Wagner, L. Samuelson, K. Deppert, and M.T. Borgström: High-performance single nanowire tunnel diodes. *Nano Lett.* **10**, 974 (2010).
70. F. Martelli, S. Rubini, M. Piccin, G. Bais, F. Jabeen, S. De Franceschi, V. Grillo, E. Carlino, F. D'Acapito, F. Boscherini, S. Cabrini, M. Lazzarino, L. Businaro, F. Romanato, and A. Franciosi: Manganese-induced growth of GaAs nanowires. *Nano Lett.* **6**, 2130 (2006).
71. T. Richter, H. Luth, T. Schapers, R. Meijers, K. Jeganathan, S.E. Hernandez, R. Calarco, and M. Marso: Electrical transport properties of single undoped and n-type doped InN nanowires. *Nanotechnology* **20**, 405206 (2009).
72. R. Cusco, N. Domenech-Amador, L. Artus, T. Gotschke, K. Jeganathan, T. Stoica, and R. Calarco: Probing the electron density in undoped, Si-doped, and Mg-doped InN nanowires by means of Raman scattering. *Appl. Phys. Lett.* **97**, 221906 (2010).
73. H.P. Song, A.L. Yang, R.Q. Zhang, Y. Guo, H.Y. Wei, G.L. Zheng, S.Y. Yang, X.L. Liu, Q.S. Zhu, and Z.G. Wang: Well-aligned Zn-doped InN nanorods grown by metal-organic chemical vapor deposition and the dopant distribution. *Cryst. Growth Des.* **9**, 3292 (2009).
74. L. Rigutti, A.D. Bugallo, M. Tchernycheva, G. Jacopin, F.H. Julien, G. Cirlin, G. Patriarche, D. Lucot, L. Travers, and J.C. Harmand: Si incorporation in InP nanowires grown by Au-assisted molecular beam epitaxy. *J. Nanomater.* **2009**, 435451 (2009).
75. H. Goto, K. Nosaki, K. Tomioka, S. Hara, K. Hiruma, J. Motohisa, and T. Fukui: growth of core–shell InP nanowires for photovoltaic application by selective-area metal organic vapor phase epitaxy. *Appl. Phys. Express* **2**, 035004 (2009).
76. X.F. Duan, Y. Huang, Y. Cui, J.F. Wang, and C.M. Lieber: Indium phosphide nanowires as building blocks for nanoscale electronic and optoelectronic devices. *Nature* **409**, 66 (2001).
77. M.T. Borgström, E. Norberg, P. Wickert, H.A. Nilsson, J. Trägårdh, K.A. Dick, G. Statkute, P. Ramvall, K. Deppert, and L. Samuelson: Precursor evaluation for in situ InP nanowire doping. *Nanotechnology* **19**, 445602 (2008).
78. M.H.M. van Weert, A. Helman, W. van den Einden, R.E. Algra, M.A. Verheijen, M.T. Borgström, G. Immink, J.J. Kelly, L.P. Kouwenhoven, and E.P.A.M. Bakkers: Zinc incorporation via the vapor-liquid-solid mechanism into InP nanowires. *J. Am. Chem. Soc.* **131**, 4578 (2009).
79. J. Wallentin, K. Mergenthaler, M. Ek, L.R. Wallenberg, L. Samuelson, K. Deppert, M.-E. Pistol, and M.T. Borgström: Probing the wurtzite conduction band structure using state-filling in highly doped InP nanowires. *Nano Lett.* **11,** 2286 (2011).
80. S. De Franceschi, J.A. van Dam, E. Bakkers, L.F. Feiner, L. Gurevich, and L.P. Kouwenhoven: Single-electron tunneling in InP nanowires. *Appl. Phys. Lett.* **83**, 344 (2003).
81. C. Liu, L. Dai, L.P. You, W.J. Xu, and G.G. Qin: Blueshift of electroluminescence from single n-InP nanowire/p-Si heterojunctions due to the Burstein–Moss effect. *Nanotechnology* **19**, 465203 (2008).
82. M.H.M. van Weert, O. Wunnicke, A.L. Roest, T.J. Eijkemans, A. Yu Silov, and J.E.M. Haverkort, G.W. 't Hooft, E.P.A.M. Bakkers: Large redshift in photoluminescence of p-doped InP nanowires induced by Fermi-level pinning. *Appl. Phys. Lett.* **88**, 043109 (2006).
83. J. Wallentin, M. Ek, L.R. Wallenberg, L. Samuelson, K. Deppert, and M.T. Borgström: Changes in contact angle of seed particle correlated with increased zincblende formation in doped InP nanowires. *Nano Lett.* **10**, 4807 (2010).
84. M.T. Borgström, J. Wallentin, M. Heurlin, S. Fält, P. Wickert, J. Leene, M.H. Magnusson, K. Deppert, and L. Samuelson: Nanowires With Promise for Photovoltaics. *IEEE Journal of Selected Topics in Quantum Electronics* **17**, 1050 (2011).
85. C. Thelander, K.A. Dick, M.T. Borgström, L.E. Fröberg, P. Caroff, H.A. Nilsson, and L. Samuelson: The electrical and structural properties of n-type InAs nanowires grown from metal-organic precursors. *Nanotechnology* **21**, 205703 (2010).
86. B.S. Sorensen, M. Aagesen, C.B. Sorensen, P.E. Lindelof, K.L. Martinez, and J. Nygard: Ambipolar transistor behavior in p-doped InAs nanowires grown by molecular beam epitaxy. *Appl. Phys. Lett.* **92**, 012119 (2008).
87. B.Y. Geng, G.Z. Wang, Z. Jiang, T. Xie, S.H. Sun, G.W. Meng, and L.D. Zhang: Synthesis and optical properties of S-doped ZnO nanowires. *Appl. Phys. Lett.* **82**, 4791 (2003).
88. S.Y. Bae, H.W. Seo, and J.H. Park: Vertically aligned sulfur-doped ZnO nanowires synthesized via chemical vapor deposition. *J. Phys. Chem. B* **108**, 5206 (2004).
89. S.Y. Li, P. Lin, C.Y. Lee, T.Y. Tseng, and C.J. Huang: Effect of Sn dopant on the properties of ZnO nanowires. *J. Phys. D* **37**, 2274 (2004).

https://doi.org/10.1557/jmr.2011.214 Published online by Cambridge University Press

90. J.Y. Gao, X.Z. Zhang, Y.H. Sun, Q. Zhao, and D.P. Yu: Compensation mechanism in N-doped ZnO nanowires. *Nanotechnology* **21**, 245703 (2010).
91. G.D. Yuan, W.J. Zhang, J.S. Jie, X. Fan, J.X. Tang, I. Shafiq, Z.Z. Ye, C.S. Lee, and S.T. Lee: Tunable n-type conductivity and transport properties of Ga-doped ZnO nanowire arrays. *Adv. Mater.* **20**, 168 (2008).
92. C.H. Liu, W.C. Yiu, F.C.K. Au, J.X. Ding, C.S. Lee, and S.T. Lee: Electrical properties of zinc oxide nanowires and intramolecular p-n junctions. *Appl. Phys. Lett.* **83**, 3168 (2003).
93. B. Xiang, P.W. Wang, X.Z. Zhang, S.A. Dayeh, D.P.R. Aplin, C. Soci, D.P. Yu, and D.L. Wang: Rational synthesis of p-type zinc oxide nanowire arrays using simple chemical vapor deposition. *Nano Lett.* **7**, 323 (2007).
94. P.J. Li, Z.M. Liao, X.Z. Zhang, X.J. Zhang, H.C. Zhu, J.Y. Gao, K. Laurent, Y. Leprince-Wang, N. Wang, and D.P. Yu: Electrical and photoresponse properties of an intramolecular p-n homojunction in single phosphorus-doped ZnO nanowires. *Nano Lett.* **9**, 2513 (2009).
95. G.D. Yuan, W.J. Zhang, J.S. Jie, X. Fan, J.A. Zapien, Y.H. Leung, L.B. Luo, P.F. Wang, C.S. Lee, and S.T. Lee: P-type ZnO nanowire arrays. *Nano Lett.* **8**, 2591 (2008).
96. W. Liu, F.X. Xiu, K. Sun, Y.H. Xie, K.L. Wang, Y. Wang, J. Zou, Z. Yang, and J.L. Liu: Na-doped p-type ZnO microwires. *J. Am. Chem. Soc.* **132**, 2498 (2010).
97. Y.Q. Chang, D.B. Wang, X.H. Luo, X.Y. Xu, X.H. Chen, L. Li, C.P. Chen, R.M. Wang, J. Xu, and D.P. Yu: Synthesis, optical, and magnetic properties of diluted magnetic semiconductor $Zn_{1-x}Mn_xO$ nanowires via vapor phase growth. *Appl. Phys. Lett.* **83**, 4020 (2003).
98. J.J. Liu, M.H. Yu, and W.L. Zhou: Well-aligned Mn-doped ZnO nanowires synthesized by a chemical-vapor-deposition method. *Appl. Phys. Lett.* **87**, 172505 (2005).
99. P.V. Radovanovic, C.J. Barrelet, S. Gradecak, F. Qian, and C.M. Lieber: General synthesis of manganese-doped II-VI and III-V semiconductor nanowires. *Nano Lett.* **5**, 1407 (2005).
100. M. Willander, O. Nur, Q.X. Zhao, L.L. Yang, M. Lorenz, B.Q. Cao, J.Z. Perez, C. Czekalla, G. Zimmermann, M. Grundmann, A. Bakin, A. Behrends, M. Al-Suleiman, A. El-Shaer, A.C. Mofor, B. Postels, A. Waag, N. Boukos, A. Travlos, H.S. Kwack, J. Guinard, and D.L. Dang: Zinc oxide nanorod based photonic devices: Recent progress in growth, light emitting diodes and lasers. *Nanotechnology* **20**, 332001 (2009).
101. Z.Y. Fan and J.G. Lu: Zinc oxide nanostructures: Synthesis and properties. *J. Nanosci. Nanotechnol* **5**, 1561 (2005).
102. Y.Q. Chen, J. Jiang, B. Wang, and J.G. Hou: Synthesis of tin-doped indium oxide nanowires by self-catalytic VLS growth. *J. Phys. D: Appl. Phys.* **37**, 3319 (2004).
103. Q. Wan, Z.T. Song, S.L. Feng, and T.H. Wang: Single-crystalline tin-doped indium oxide whiskers: Synthesis and characterization. *Appl. Phys. Lett.* **85**, 4759 (2004).
104. Q. Wan, E.N. Dattoli, W.Y. Fung, W. Guo, Y.B. Chen, X.Q. Pan, and W. Lu: High-performance transparent conducting oxide nanowires. *Nano Lett.* **6**, 2909 (2006).
105. P. Nguyen, H.T. Ng, J. Kong, A.M. Cassell, R. Quinn, J. Li, J. Han, M. McNeil, and M. Meyyappan: Epitaxial directional growth of indium-doped tin oxide nanowire arrays. *Nano Lett.* **3**, 925 (2003).
106. Q. Wan, E.N. Dattoli, and W. Lu: Transparent metallic Sb-doped SnO2 nanowires. *Appl. Phys. Lett.* **90**, 222107 (2007).
107. A. Klamchuen, T. Yanagida, K. Nagashima, S. Seki, K. Oka, M. Taniguchi, and T. Kawai: Crucial role of doping dynamics on transport properties of Sb-doped SnO2 nanowires. *Appl. Phys. Lett.* **95**, 053105 (2009).
108. J.S. Jie, W.J. Zhang, I. Bello, C.S. Lee, and S.T. Lee: One-dimensional II-VI nanostructures: Synthesis, properties and optoelectronic applications. *Nano Today* **5**, 313 (2010).
109. B.A. Wacaser, K.A. Dick, J. Johansson, M.T. Borgström, K. Deppert, and L. Samuelson: Preferential interface nucleation: An expansion of the VLS growth mechanism for nanowires. *Adv. Mater.* **21**, 153 (2009).
110. K.A. Dick: A review of nanowire growth promoted by alloys and non-alloying elements with emphasis on Au-assisted III-V nanowires. *Prog. Cryst. Growth Charact. Mater.* **54**, 138 (2008).
111. J.E. Allen, D.E. Perea, E.R. Hemesath, and L.J. Lauhon: Nonuniform nanowire doping profiles revealed by quantitative scanning photocurrent microscopy. *Adv. Mater.* **21**, 3067 (2009).
112. M.A. Verheijen, G. Immink, T. de Smet, M.T. Borgström, and E.P.A.M. Bakkers: Growth kinetics of heterostructured GaP–GaAs nanowires. *J. Am. Chem. Soc.* **128**, 1353 (2006).
113. M.T. Borgström, J. Wallentin, J. Trägårdh, P. Ramvall, M. Ek, L.R. Wallenberg, L. Samuelson, and K. Deppert: In situ etching for total control over axial and radial nanowire growth. *Nano Research* **3**, 264 (2010).
114. E. Kuphal: Preparation and characterization of LPE InP. *J. Cryst. Growth* **54**, 117 (1981).
115. R.A. Logan, T. Tanbunek, and A.M. Sergent: Doping of InP and GaInAs with S during metalorganic vapor phase epitaxy. *J. Appl. Phys.* **65**, 3723 (1989).
116. N. Li, T.Y. Tan, and U. Gösele: Transition region width of nanowire hetero- and pn-junctions grown using vapor–liquid–solid processes. *Appl. Phys. A* **90**, 591 (2008).
117. M.T. Björk, B.J. Ohlsson, T. Sass, A.I. Persson, C. Thelander, M.H. Magnusson, K. Deppert, L.R. Wallenberg, and L. Samuelson: One-dimensional heterostructures in semiconductor nanowhiskers. *Appl. Phys. Lett.* **80**, 1058 (2002).
118. M.T. Borgström, M.A. Verheijen, G. Immink, T. de Smet, and E.P.A.M. Bakkers: Interface study on heterostructured GaP–GaAs nanowires. *Nanotechnology* **17**, 4010 (2006).
119. L.E. Fröberg, B.A. Wacaser, J.B. Wagner, S. Jeppesen, B.J. Ohlsson, K. Deppert, and L. Samuelson: Transients in the formation of nanowire heterostructures. *Nano Lett.* **8**, 3815 (2008).
120. C.Y. Wen, M.C. Reuter, J. Bruley, J. Tersoff, S. Kodambaka, E.A. Stach, and F.M. Ross: Formation of compositionally abrupt axial heterojunctions in silicon-germanium nanowires. *Science* **326**, 1247 (2009).
121. F. Glas, J-C. Harmand, and G. Patriarche: Nucleation antibunching in catalyst-assisted nanowire growth. *Phys. Rev. Lett.* **104**, 135501 (2010).
122. H. Peelaers, B. Partoens, and F.M. Peeters: Formation and segregation energies of B and P doped and BP codoped silicon nanowires. *Nano Lett.* **6**, 2781 (2006).
123. M.V. Fernandez-Serra, C. Adessi, and X. Blase: Surface segregation and backscattering in doped silicon nanowires. *Phys. Rev. Lett.* **96**, 166805 (2006).
124. P. Xie, Y.J. Hu, Y. Fang, J.L. Huang, and C.M. Lieber: Diameter-dependent dopant location in silicon and germanium nanowires. *Proc. Natl. Acad. Sci. USA* **106**, 15254 (2009).
125. J. Johansson, L.S. Karlsson, C.P.T. Svensson, T. Mårtensson, B.A. Wacaser, K. Deppert, L. Samuelson, and W. Seifert: Structural properties of (111)B-oriented III-V nanowires. *Nat. Mater.* **5**, 574 (2006).
126. S. Chichibu, M. Kushibe, K. Eguchi, M. Funemizu, and Y. Ohba: High-concentration Zn doping in Inp grown by low-pressure metal-organic chemical vapor-deposition. *J. Appl. Phys.* **68**, 859 (1990).
127. M. Diarra, Y.M. Niquet, C. Delerue, and G. Allan: Ionization energy of donor and acceptor impurities in semiconductor nanowires: Importance of dielectric confinement. *Phys. Rev. B* **75**, 045301 (2007).
128. M.T. Björk, H. Schmid, J. Knoch, H. Riel, and W. Riess: Donor deactivation in silicon nanostructures. *Nat. Nanotechnol.* **4**, 103 (2009).

https://doi.org/10.1557/jmr.2011.214 Published online by Cambridge University Press

129. K-H. Hong, J. Kim, J.H. Lee, J. Shin, and U.I. Chung: Asymmetric doping in silicon nanostructures: the impact of surface dangling bonds. *Nano Lett.* **10**, 1671 (2010).
130. J. Arbiol, S. Estrade, J.D. Prades, A. Cirera, F. Furtmayr, C. Stark, A. Laufer, M. Stutzmann, M. Eickhoff, M.H. Gass, A.L. Bleloch, F. Peiro, and J.R. Morante: Triple-twin domains in Mg doped GaN wurtzite nanowires: Structural and electronic properties of this zinc-blende-like stacking. *Nanotechnology* **20**, 145704 (2009).
131. B.D. Liu, Y. Bando, C.C. Tang, F.F. Xu, and D. Golberg: Excellent field-emission properties of P-doped GaN nanowires. *J. Phys. Chem. B* **109**, 21521 (2005).
132. A.C. Ford, S. Chuang, J.C. Ho, Y.L. Chueh, Z.Y. Fan, and A. Javey: Patterned p-doping of InAs nanowires by gas-phase surface diffusion of Zn. *Nano Lett.* **10**, 509 (2010).
133. K.E. Moselund, H. Ghoneim, H. Schmid, M.T. Björk, E. Lortscher, S. Karg, G. Signorello, D. Webb, M. Tschudy, R. Beyeler, and H. Riel: Solid-state diffusion as an efficient doping method for silicon nanowires and nanowire field effect transistors. *Nanotechnology* **21**, 435202 (2010).
134. J.C. Ho, R. Yerushalmi, Z.A. Jacobson, Z. Fan, R.L. Alley, and A. Javey: Controlled nanoscale doping of semiconductors via molecular monolayers. *Nat. Mater.* **7**, 62 (2008).
135. S. Dhara, A. Datta, C.T. Wu, Z.H. Lan, K.H. Chen, Y.L. Wang, Y.F. Chen, C.W. Hsu, L.C. Chen, H.M. Lin, and C.C. Chen: Blueshift of yellow luminescence band in self-ion-implanted n-GaN nanowire. *Appl. Phys. Lett.* **84**, 3486 (2004).
136. O. Hayden, M.T. Björk, H. Schmid, H. Riel, U. Drechsler, S.F. Karg, E. Lortscher, and W. Riess: Fully depleted nanowire field-effect transistor in inversion mode. *Small* **3**, 230 (2007).
137. G.M. Cohen, M.J. Rooks, J.O. Chu, S.E. Laux, P.M. Solomon, J.A. Ott, R.J. Miller, and W. Haensch: Nanowire metal-oxide-semiconductor field effect transistor with doped epitaxial contacts for source and drain. *Appl. Phys. Lett.* **90**, 233110 (2007).
138. D. Stichtenoth, K. Wegener, C. Gutsche, I. Regolin, F.J. Tegude, W. Prost, M. Seibt, and C. Ronning: P-type doping of GaAs nanowires. *Appl. Phys. Lett.* **92**, 163107 (2008).
139. A. Colli, A. Fasoli, C. Ronning, S. Pisana, S. Piscanec, and A.C. Ferrari: Ion beam doping of silicon nanowires. *Nano Lett.* **8**, 2188 (2008).
140. P. Das Kanungo, R. Kögler, K. Nguyen-Duc, N. Zakharov, P. Werner, and U. Gösele: Ex situ n and p doping of vertical epitaxial short silicon nanowires by ion implantation. *Nanotechnology* **20**, 165706 (2009).
141. S. Hoffmann, J. Bauer, C. Ronning, T. Stelzner, J. Michler, C. Ballif, V. Sivakov, and S.H. Christiansen: Axial p-n junctions realized in silicon nanowires by ion implantation. *Nano Lett.* **9**, 1341 (2009).
142. H.Y. Li, O. Wunnicke, M.T. Borgström, W.G.G. Immink, M.H.M. van Weert, M.A. Verheijen, and E. Bakkers: Remote p-doping of InAs nanowires. *Nano Lett.* **7**, 1144 (2007).
143. J. Simon, V. Protasenko, C. Lian, H. Xing, and D. Jena: Polarization-induced hole doping in wide-band-gap uniaxial semiconductor heterostructures. *Science* **327**, 60 (2010).
144. F. Boxberg, N. Søndergaard, and H.Q. Xu: Photovoltaics with piezoelectric core-shell nanowires. *Nano Lett.* **10**, 1108 (2010).
145. J.R. Kim, B.K. Kim, I.J. Lee, J.J. Kim, J. Kim, S.C. Lyu, and C.J. Lee: Temperature-dependent single-electron tunneling effect in lightly and heavily doped GaN nanowires. *Phys. Rev. B* **69**, 233303 (2004).
146. E. Stern, G. Cheng, E. Cimpoiasu, R. Klie, S. Guthrie, J. Klemic, I. Kretzschmar, E. Steinlauf, D. Turner-Evans, E. Broomfield, J. Hyland, R. Koudelka, T. Boone, M. Young, A. Sanders, R. Munden, T. Lee, D. Routenberg, and M.A. Reed: Electrical characterization of single GaN nanowires. *Nanotechnology* **16**, 2941 (2005).
147. S. Sze: *Physics of Semiconductor Devices* (Wiley, New York, 1981).
148. P.M. Morse and H. Feshbach: *Methods of Theoretical Physics* (McGraw-Hill, New York, 1953).
149. H.T. Ng, J. Han, T. Yamada, P. Nguyen, Y.P. Chen, and M. Meyyappan: Single crystal nanowire vertical surround-gate field-effect transistor. *Nano Lett.* **4**, 1247 (2004).
150. O. Wunnicke: Gate capacitance of back-gated nanowire field-effect transistors. *Appl. Phys. Lett.* **89**, 083102 (2006).
151. D.R. Khanal and J. Wu: Gate coupling and charge distribution in nanowire field effect transistors. *Nano Lett.* **7**, 2778 (2007).
152. A.V. Kretinin, R. Popovitz-Biro, D. Mahalu, and H. Shtrikman: Multimode Fabry-Perot conductance oscillations in suspended stacking-faults-free InAs nanowires. *Nano Lett.* **10**, 3439 (2010).
153. H. Park, R. Beresford, S. Hong, and J. Xu: Geometry- and size-dependence of electrical properties of metal contacts on semiconducting nanowires. *J. Appl. Phys.* **108**, 094308 (2010).
154. D.G. Ivey, P. Jian, L. Wan, R. Bruce, S. Eicher, and C. Blaauw: Pd/Zn/Pd/Au ohmic contacts to p-type Inp. *J. Electron. Mater.* **20**, 237 (1991).
155. Y. Cui, Z.H. Zhong, D.L. Wang, W.U. Wang, and C.M. Lieber: High performance silicon nanowire field effect transistors. *Nano Lett.* **3**, 149 (2003).
156. Y. Huang, X. Duan, Y. Cui, and C.M. Lieber: Gallium nitride nanowire nanodevices. *Nano Lett.* **2**, 101 (2002).
157. F. Leonard and A.A. Talin: Size-dependent effects on electrical contacts to nanotubes and nanowires. *Phys. Rev. Lett.* **97**, 026804 (2006).
158. C. Thelander, M.T. Björk, M.W. Larsson, A.E. Hansen, L.R. Wallenberg, and L. Samuelson: Electron transport in InAs nanowires and heterostructure nanowire devices. *Solid State Commun.* **131**, 573 (2004).
159. Z.Y. Zhang, K. Yao, Y. Liu, C.H. Jin, X.L. Liang, Q. Chen, and L.M. Peng: Quantitative analysis of current-voltage characteristics of semiconducting nanowires: Decoupling of contact effects. *Adv. Funct. Mater.* **17**, 2478 (2007).
160. W.M. Weber, L. Geelhaar, E. Unger, C. Cheze, F. Kreupl, H. Riechert, and P. Lugli: Silicon to nickel-silicide axial nanowire heterostructures for high performance electronics. *Phys. Status Solidi B Basic Res.* **244**, 4170 (2007).
161. R. Tu, L. Zhang, Y. Nishi, and H.J. Dai: Measuring the capacitance of individual semiconductor nanowires for carrier mobility assessment. *Nano Lett.* **7**, 1561 (2007).
162. S. Roddaro, K. Nilsson, G. Astromskas, L. Samuelson, L.E. Wernersson, O. Karlström, and A. Wacker: InAs nanowire metal-oxide-semiconductor capacitors. *Appl. Phys. Lett.* **92**, 253509 (2008).
163. O. Karlström, A. Wacker, K. Nilsson, G. Astromskas, S. Roddaro, L. Samuelson, and L.E. Wernersson: Analysing the capacitance-voltage measurements of vertical wrapped-gated nanowires. *Nanotechnology* **19**, 435201 (2008).
164. G. Astromskas, K. Storm, O. Karlström, P. Caroff, M. Borgström, and L-E. Wernersson: Doping incorporation in InAs nanowires characterized by capacitance measurements. *J. Appl. Phys.* **108**, 054306 (2010).
165. E.C. Garnett, Y.C. Tseng, D.R. Khanal, J.Q. Wu, J. Bokor, and P.D. Yang: Dopant profiling and surface analysis of silicon nanowires using capacitance-voltage measurements. *Nat. Nanotechnol.* **4**, 311 (2009).
166. E.P.A.M. Bakkers, J.A. Van Dam, S. De Franceschi, L.P. Kouwenhoven, M. Kaiser, M. Verheijen, H. Wondergem, and P. Van der Sluis: Epitaxial growth of InP nanowires on germanium. *Nat. Mater.* **3**, 769 (2004).

https://doi.org/10.1557/jmr.2011.214 Published online by Cambridge University Press

167. M. Bugajski and W. Lewandowski: Concentration-dependent absorption and photoluminescence of n-type InP. *J. Appl. Phys.* **57**, 521 (1985).
168. T. Kawashima, G. Imamura, T. Saitoh, K. Komori, M. Fujii, and S. Hayashi: Raman scattering studies of electrically active impurities in in situ B-Doped silicon nanowires: Effects of annealing and oxidation. *J. Phys. Chem. C* **111**, 15160 (2007).
169. K. Jeganathan, R.K. Debnath, R. Meijers, T. Stoica, R. Calarco, D. Grutzmacher, and H. Luth: Raman scattering of phonon-plasmon coupled modes in self-assembled GaN nanowires. *J. Appl. Phys.* **105**, 123707 (2009).
170. P. Parkinson, H.J. Joyce, Q. Gao, H.H. Tan, X. Zhang, J. Zou, C. Jagadish, L.M. Herz, and M.B. Johnston: Carrier lifetime and mobility enhancement in nearly defect-free core-shell nanowires measured using time-resolved terahertz spectroscopy. *Nano Lett.* **9**, 3349 (2009).
171. T. Richter, H. Luth, R. Meijers, R. Calarco, and M. Marso: doping concentration of gan nanowires determined by opto-electrical measurements. *Nano Lett.* **8**, 3056 (2008).
172. N.A. Sanford, P.T. Blanchard, K.A. Bertness, L. Mansfield, J.B. Schlager, A.W. Sanders, A. Roshko, B.B. Burton, and S.M. George: Steady-state and transient photoconductivity in *c*-axis GaN nanowires grown by nitrogen-plasma-assisted molecular-beam epitaxy. *J. Appl. Phys.* **107**, 034318 (2010).
173. M.C. Putnam, M.A. Filler, B.M. Kayes, M.D. Kelzenberg, Y.B. Guan, N.S. Lewis, J.M. Eiler, and H.A. Atwater: Secondary ion mass spectrometry of vapor-liquid-solid grown, Au-catalyzed, Si wires. *Nano Lett.* **8**, 3109 (2008).
174. D.E. Perea, J.E. Allen, S.J. May, B.W. Wessels, D.N. Seidman, and L.J. Lauhon: Three-dimensional nanoscale composition mapping of semiconductor nanowires. *Nano Lett.* **6**, 181 (2006).
175. J.E. Allen, E.R. Hemesath, D.E. Perea, J.L. Lensch-Falk, Z.Y. Li, F. Yin, M.H. Gass, P. Wang, A.L. Bleloch, R.E. Palmer, and L.J. Lauhon: High-resolution detection of Au catalyst atoms in Si nanowires. *Nat. Nanotechnol.* **3**, 168 (2008).
176. T. Xu, J.P. Nys, B. Grandidier, D. Stievenard, Y. Coffinier, R. Boukherroub, R. Larde, E. Cadel, and P. Pareige: Growth of Si nanowires on micropillars for the study of their dopant distribution by atom probe tomography. *J. Vac. Sci. Technol., B* **26**, 1960 (2008).
177. D.E. Perea, J.L. Lensch, S.J. May, B.W. Wessels, and L.J. Lauhon: Composition analysis of single semiconductor nanowires using pulsed-laser atom probe tomography. *Appl. Phys. A* **85**, 271 (2006).
178. T.J. Prosa, R. Alvis, L. Tsakalakos, and V.S. Smentkowski: Characterization of dilute species within CVD-grown silicon nanowires doped using trimethylboron: Protected lift-out specimen preparation for atom probe tomography. *J. Microsc. (Oxf.)* **239**, 92 (2010).
179. L.J. Lauhon, P. Adusumilli, P. Ronsheim, P.L. Flaitz, and D. Lawrence: Atom-probe tomography of semiconductor materials and device structures. *MRS Bull.* **34**, 738 (2009).
180. D.D.D. Ma, C.S. Lee, and S.T. Lee: Scanning tunneling microscopic study of boron-doped silicon nanowires. *Appl. Phys. Lett.* **79**, 2468 (2001).
181. C. Yang, Z.H. Zhong, and C.M. Lieber: Encoding electronic properties by synthesis of axial modulation-doped silicon nanowires. *Science* **310**, 1304 (2005).
182. S. Vinaji, A. Lochthofen, W. Mertin, I. Regolin, C. Gutsche, W. Prost, F.J. Tegude, and G. Bacher: Material and doping transitions in single GaAs-based nanowires probed by Kelvin probe force microscopy. *Nanotechnology* **20**, 385702 (2009).
183. E. Koren, N. Berkovitch, and Y. Rosenwaks: Measurement of active dopant distribution and diffusion in individual silicon nanowires. *Nano Lett.* **10**, 1163 (2010).
184. X. Ou, P. Das Kanungo, R. Kögler, P. Werner, U. Gösele, W. Skorupa, and X. Wang: Carrier profiling of individual Si nanowires by scanning spreading resistance microscopy. *Nano Lett.* **10**, 171 (2010).
185. J.M. Stiegler, A.J. Huber, S.L. Diedenhofen, J.G. Rivas, R.E. Algra, E. Bakkers, and R. Hillenbrand: Nanoscale free-carrier profiling of individual semiconductor nanowires by infrared near-field nanoscopy. *Nano Lett.* **10**, 1387 (2010).
186. X.F. Wang, F.Q. Song, Q. Chen, T.Y. Wang, J.L. Wang, P. Liu, M.R. Shen, J.G. Wan, G.H. Wang, and J.B. Xu: Scaling dopant states in a semiconducting nanostructure by chemically resolved electron energy-loss spectroscopy: a case study on Co-Doped ZnO. *J. Am. Chem. Soc.* **132**, 6492 (2010).
187. X.C. Jiang, Q.H. Xiong, S. Nam, F. Qian, Y. Li, and C.M. Lieber: InAs/InP radial nanowire heterostructures as high electron mobility devices. *Nano Lett.* **7**, 3214 (2007).

https://doi.org/10.1557/jmr.2011.214 Published online by Cambridge University Press